Monitoring Oyster Restoration Reefs in the Great Wicomico, Piankatank and Lynnhaven Rivers Part II – Great Wicomico River

Great Wicomico River

Romuald N. Lipcius, Russell P. Burke and Gabrielle G. Saluta

23 December 2020

Contents

1 Inside Cover

CHESAPEAKE WATERSHED CESU
W912HZ-18-SOI-0006

MONITORING OYSTER RESTORATION REEFS IN THE GREAT WICOMICO, PIANKATANK AND LYNNHAVEN RIVERS

FINAL REPORT: PART II - GREAT WICOMICO RIVER*

Principal Investigator: Romuald N. Lipcius, Ph.D.
Virginia Institute of Marine Science, William & Mary
Gloucester Point, Virginia 23062

Co-Principal Investigator: Russell P. Burke, Ph.D.
Department of Organismal and Environmental Biology
Christopher Newport University
Newport News, Virginia

Marine Scientist: Gabrielle G. Saluta, M.S.
Virginia Institute of Marine Science, William & Mary
Gloucester Point, Virginia 23062

23 December 2020

* Citation: Lipcius, Romuald N., Burke, Russell P. and Saluta, Gabrielle G. 2020. Monitoring Oyster Restoration Reefs in the Great Wicomico, Piankatank and Lynnhaven Rivers. Chesapeake Watershed CESU W912HZ-18-SOI-0006 Final Report: Part II - Great Wicomico River. US Army Corps of Engineers, Norfolk, Virginia.

2 Summary

We assessed the performance of reefs constructed in 2004 by USACE in the Great Wicomico River in 2018 and 2019, 15 y after construction. Monitoring objectives included assessing abundance and biomass, oyster demographics (live and dead) including age classes, and accretion rates on the restored reefs. Generalized linear models were used to analyze 6 response variables: spat density, adult density, total density, biomass, live shell volume and brown shell volume. Independent variables included water depth as a continuous variable, sediment type (mud or muddy sand) as a categorical factor, and reef type (Original High-Relief Reef, OHRR; Rehabilitated High-Relief Reef, RHRR; and Original Low-Relief Reef, OLRR) as a categorical factor. Nine statistical models representing alternative hypotheses were developed to analyze the 6 response variables as a function of water depth, sediment type and reef type, and the best model was selected using Information Theory with Akaike's Information Criterion. In addition, we analyzed the relationship between spat density on oyster patches as a function of adult density.

Sanctuary reefs in the Great Wicomico River (GWR) have performed exceptionally well over the past 15 years, except for a few sites that have been poached or where reef was originally constructed on poor habitat, specifically deep mud bottom. Oyster size ranged from 3.1 to 132.2 mm SH (Shell Height = Shell Length) with most oysters being 40 to 90 mm SH. Larger oysters comprised at least 2 to 3 year classes.

Spat density was low due to poor recruitment in 2018, inversely related to depth and higher in muddy sand than in mud, but did not differ significantly by reef type. Spat density was highest on OHRR at 43.1 m^{-2} on OHRR, intermediate on RHRR at 31.2 m^{-2}, and lowest on OLRR at 27.2 m^{-2}. The lack of a reef type effect resulted from the extremely poor spat set of 2018, which was due to high streamflow in 2018, and which precluded accumulation of spat on OHRR and RHRR reefs. This was also evident in the high volume of brown shell without spat.

Adult and total density were high in 2018 and 2019, also inversely related to depth and higher in muddy sand than in mud, though depth interacted significantly with reef type. OHRR reefs had a steeper negative slope than RHRR and OLRR reefs, such that the difference in density between OHRR and the other reef types was greatest at depths shallower than 12 feet; by 16

feet in depth, density was relatively low and differed little among the 3 reef types. This was likely due to the negative effect of depth on spat recruitment in combination with effects of reef height on recruitment and survival.

To assess population-level differences in oyster density, we first determined whether depth differed by reef type. It did not, which allowed us to generate mean population-level densities as a function of reef type. In contrast to spat density, both adult density and total density differed significantly by reef type. OHRR supported the highest densities (adult: 258.9 m^{-2}; total: 301.0 m^{-2}), followed by RHRR (adult: 151.8 m^{-2}; total: 182.0 m^{-2}), and OLRR with the lowest (adult: 91.7 m^{-2}; total: 118.0 m^{-2}), though all reef types greatly exceeded the GIT target of 50 oysters m^{-2}. Spat density was significantly and positively correlated with adult density.

Total oyster biomass was high in 2018 and 2019, also inversely related to depth and higher in muddy sand than in mud, though depth interacted significantly with reef type. As with adult and total oyster densities, OHRR reefs had a steeper negative slope than RHRR and OLRR reefs, such that the difference in biomass between OHRR and the other reef types was greatest at depths shallower than 12 feet; from 12 to 16 feet in depth, biomass declined and differed little among the 3 reef types. Given that depth did not differ by reef type, we generated mean population-level biomass as a function of reef type. OHRR harbored highest total biomass (173.0 g dry weight (DW) m^{-2}), RHRR was nearly as high (164.0 g DW m^{-2}), whereas OLRR was substantially lower (57.0 g DW m^{-2}), though all reef types exceeded the GIT target of 50 g DW m^{-2}.

Live shell volume was high in 2018 and 2019, inversely related to depth and higher in muddy sand than in mud; depth again interacted significantly with reef type. As with adult density, total oyster density and biomass, OHRR reefs had a steeper negative slope than RHRR and OLRR reefs, such that the difference in live shell volume between OHRR and the other reef types was greatest at depths shallower than 12 feet. In contrast, brown shell volume was positively related to depth, did not differ by sediment type, and depth did not interact with reef type such that RHRR reefs had the highest volume of brown shell. The change in slope with depth from negative for live shell volume to positive for brown shell volume resulted from the reduction of spat and adult densities with depth, as well as the addition of RHRR shell during reef rehabilitation.

Again, given that depth did not differ by reef type, we generated mean population-level live shell volume and brown shell volume as a function of reef type. Live shell volume differed significantly by reef type. OHRR harbored highest live shell volume (8.302 L m^{-2}), RHRR was intermediate (6.650 L m^{-2}), whereas OLRR was substantially lower (2.657 L m^{-2}). Conversely, brown shell volume was highest on RHRR (16.537 L m^{-2}), followed by OHRR (12.843 L m^{-2}) and then OLRR with lowest volumes (10.638 L m^{-2}). When live shell volume and brown shell volume were combined by reef type, all reef types exceeded an assumed value for self-sustaining reefs of 5 L m^{-2}.

Given that multiple year classes inhabited the reef network, and that density and biomass exceeded GIT metrics, we conclude that all GWR reefs are performing successfully. In addition, the high volume of live oysters and brown shell are indicative of positively accreting reefs.

Population abundance across all reef types was estimated at 76.2 million live oysters, most of which were adults. Of all oysters, OHRR reefs harbored 36.3 million, RHRR reefs 22.0 million, and OLRR reefs 17.9 million.

Poaching was evident on 6 of the 64 samples across the reef network with 3 on reef 8, 2 on reef 9 and 1 on reef 3. We identified poached samples by the occurrence of profuse broken shell pieces and lack of large oysters either live or dead (boxes). In unpoached samples, legal-size oysters comprised a substantial portion of the population, whereas in poached samples very few oysters were of legal size. Poached samples also greatly reduced the number of oysters in clusters.

In summary, multiple year classes inhabited the reef network, and density and biomass greatly exceeded GIT metrics. Consequently, the GWR reef network exceeded restoration reef performance metrics established by the GIT. Accretion rates of live and brown oyster shell volume were well above those necessary for long-term, self-sustaining oyster populations. Despite poaching on some reefs and low spat densities reflecting poor recruitment in 2018, the sanctuary oyster reef network remains self-sustaining and resilient due to high densities of adults, biomass and accreted shell volume. Adaptive management whereby poorly-performing reefs were rehabilitated was successful and raised the quality of those reefs to be self-sustaining. The sanctuary oyster reef network harbors the longest-lasting (15 years) self-sustaining restored oyster metapopulation of any native oyster species worldwide, and serves as a model for native oyster restoration globally.

3 Preface

This report is Part II of a two-part report, and was prepared as a stand-alone document. Hence, sections of the report may repeat what was stated in Part I of the report (Lipcius et al., 2020).

4 Introduction

The native Eastern oyster *Crassostrea virginica* and its habitat have been severely depleted in Chesapeake Bay, as in many other regions of the world (Beck et al., 2011). Current populations in the Bay are estimated at approximately 1% (Wilberg et al., 2011) and while a limited recovery of the wild fishery is occurring at present, the overall recovery of the oyster stocks, fishery and associated reef habitat has been limited by poor habitat quality, low stock and continued low recruitment when compared to historical levels (Rothschild et al., 1994; Schulte, 2017). An aggressive restoration effort was undertaken by the U.S. Army Corps of Engineers (USACE) as part of a larger commitment to restore the Chesapeake Bay ecosystem in response to the Executive Order by President Obama in 2009. For oysters, more specific goals were established with the 2014 Chesapeake Bay Agreement, which requires 10 tributary rivers be restored by 2025. The Chesapeake Bay Program Goal Implementation Team (GIT) established standard reef location, abundance and biomass metrics to be applied at reef sites to monitor their status and assess their success over time. The USACE is a member of the GIT and has adopted the GIT standard metrics to assess the status of constructed reefs.

A large-scale, multi-agency team involving both federal and state agencies as well as academia has been conducting large-scale oyster restoration projects in both Maryland and Virginia waters of the Bay and its tributaries. Tributaries were prioritized according to their chance for success of a large-scale restoration project. Goals include: significant stock enhancement, expansion of oyster reef habitat, enhanced oyster recruitment, establishment of a network of sanctuary oyster reefs free from oyster fishing pressure, improvements to local ecology including secondary production, Submerged Aquatic Vegetation (SAV) expansion and water quality improvement, and enhancement of the oyster fishery in areas set aside for the fishery. As part of the Chesapeake Bay Native Oyster Recovery Project, the USACE constructed a

subtidal granite reef at the Piankatank River and subtidal shell reefs at the Lynnhaven River and the Great Wicomico River.

This report deals with the restoration reefs in the Great Wicomico River, which is the first major tributary on the western shore of the Bay south of the Potomac River. USACE reefs in the Great Wicomico River were sampled in 2006-2007, and again in six different years spanning 2008 through 2017. We established the protocol for effective and efficient sampling of restoration reefs with patent tong gear; validated the method with underwater remotely operated vehicle (ROV) video observations, and determined the efficiency of patent tong gear (Schulte et al., 2018). A Habitat Suitability Index was generated for oyster reef restoration in the Great Wicomico River (Theuerkauf and Lipcius, 2016).

5 Objectives

In this report, we assessed the performance of reefs constructed by USACE in the Great Wicomico River (Figure 1). Monitoring objectives included assessing abundance and biomass, oyster demographics (live and dead) including age classes, and accretion rates on the restored reefs. All work was performed in accordance with applicable local, state, and federal regulations.

The period of performance was 15 September 2018 through 14 April 2020. The original period of performance was extended due to circumstances beyond the control of the investigators. Surveys were conducted in Fall and Winter 2018, and Spring and Summer 2019. Additional video surveys were to be conducted Winter 2020, but the COVID-19 pandemic precluded their completion. As required by the contract, specific tributary sampling plans were reviewed with USACE personnel prior to the actual surveys, and adjustments made to suit USACE needs.

6 Methods

6.1 Field Survey

Reefs built by the USACE in the Great Wicomico River were sampled using a survey of randomly selected sites over the reef surface with sufficient samples to minimize the standard error of the mean (SE), an estimate of sampling precision. For the Great Wicomico River, the reefs had consisted of 2 distinct

strata, high-relief reefs (HRR) and low-relief reefs (LRR) at each of 9 reef locations (USACE reef numbers 1&2, 3, 4, 8, 9, 10&11, 13 and 16). Recently, various poorly performing LRR were refurbished to HRR status and were renamed RHRR, while the original high-relief reefs were renamed OHRR and remaining low-relief reefs were renamed OLRR. To sample the reefs, a 10-m^2 grid was drawn by the USACE over the entire reef area and assigned numbers. A random number generator computer application was used by the USACE to produce the random samples for each monitoring event. All sampling point coordinates were provided by the USACE, as well as sampling maps with the reefs sub-divided into 10 x 10 m^2 grids. Random samples were taken from a single station within each of the randomly selected 10 x 10 m^2 areas as indicated by the USACE. GPS was used during monitoring to ensure samples were taken from these points, and the exact GPS location of each station was recorded. Details of patent tong sampling methods are provided in Schulte et al. (2018).

To obtain subtidal bottom samples across the diverse bottom conditions, a commercial 'deadrise' vessel containing an oyster patent tong was employed. The captain navigated the vessel to each set of designated coordinates using a Garmin 76 GPS. Upon reaching each sample site, a large chain anchor was lowered to keep the vessel on site. The captain then lowered the patent tong to the sediment/reef surface and manipulated the tongs to ensure a deep, full grab; each grab sampled approximately one square meter of river bottom. Upon raising the sample to the surface and placement on a sorting table, but prior to any processing, a photograph was taken of the sample with a dry-erase board displaying the site information. Then, a complete 0.5 or 0.25 m^2 section of the sample was retained, cleaned of most sediment, placed in pre-labeled freezer bags, transported in a large cooler, stored in freezers at the lab at VIMS, and processed at a later date. Each sample was partitioned into two separate bags. The first bag contained all live oysters, while the second bag contained all dead shell and base shell material.

Physical variables (water clarity, temperature, salinity, dissolved oxygen) were taken at each reef. For each station within a reef, a chain anchor was deployed prior to collecting patent tong samples to ensure an accurate location with GPS. Depth and sediment type were recorded at every station.

6.2 Laboratory Processing

Laboratory processing was required because (i) spat cannot be sampled accurately in the field without a lengthy examination onboard the project vessel, and (ii) it is more cost-efficient to use the vessel time to sample, rather than both sample and process the material. Each sample was thawed and rinsed over a 1-mm sieve, enabling the removal of any excess mud and fine solids. Shell Height (SH, mm), equivalent to Shell Length, was measured using digital calipers for all live oysters, and for dead oysters both of box (both valves attached at the hinge) and of half-box (single disarticulated valve) shells. For half-box shells, only the bottom valves were measured to avoid overestimation of dead oyster density. Biomass was measured on a subset of oysters. Live oyster volume (LOV) was determined in the lab with graduated (premarked and accurate to 0.5 L) 20-L buckets or smaller graduated cylinders (accurate to 0.1 L or 0.01L), where appropriate. LOV included live oysters, dead bottom valves, and dead top valves. Dead oyster volume (DOV), containing all of the base reef material, was determined using the same water displacement procedure.

To determine biomass, soft tissue dry mass (DM = Dry Weight [DW]) from a subset of live oysters spanning the height range was used to derive reef and site specific biomass regressions (Figures 2 and 3). Simple linear regressions of $\log_{10}$DM versus $\log_{10}$SH were back-transformed to generate each equation as:

$$DM = \alpha SH^{\beta}. \tag{1}$$

The most plausible regression with the finest resolution was used. Site-specific regressions were used when sufficient individuals were available from that site to generate precise biomass estimates. If this regression was unavailable due to low numbers of oysters, a reef-specific regression was used based on individuals from the reef. If both of these regressions were unavailable due to low sample sizes, the regression based on all individuals from the Great Wicomico River was used.

Reef structure characteristics (i.e., density, biomass, and volume) were corrected for sample fraction taken, sampling efficiency (81%) and patent tong size (1.03 m^2).

6.3 Statistical Analysis

Generalized linear models using the Gamma family and log link were conducted due to the heavily right-skewed distributions of the 6 response variables: spat density (Figure 4), adult density (Figure 5), total density (Figure 6), biomass (Figure 7), live shell volume (Figure 8) and brown shell volume (Figure 9). Independent variables included water depth as a continuous variable, sediment type (mud or muddy sand) as a categorical factor, and reef type (OHRR, RHRR and OLRR) as a categorical factor.

Nine models (g_1 – g_9) were developed to analyze the 6 response variables as a function of water depth, sediment type and reef type (Table 1). Each model produced a log-likelihood value, which was then used to calculate Akaike's Information Criterion (AIC) Anderson (2008). AIC_c values were used to correct for bias due to low sample size Anderson (2008). From these, Δ_i values and model probabilities (w_i) were generated to compare the fit of the candidate models (g_i) with the model having the lowest AIC_c. A model was eliminated if its w_i was less than 0.10 Anderson (2008); the individual parameter estimates of the best model (i.e., model with the highest w_i) were then evaluated.

7 Results and Discussion

7.1 Physical Variables

Physical variables during sampling were well within the dissolved oxygen (10.8 – 14.8 mg per L), thermal (7.6 – 9.7°C) and salinity (8.0 – 8.7 [ppt]) tolerance of the Eastern oyster (Theuerkauf and Lipcius, 2016). Salinity was extremely low in 2018 through mid-2019 due to abnormally high streamflow. Water depth ranged from 1.4 – 6.6 m and Secchi depth from 1.4 - 2.6 m. Shallow Secchi depth readings corresponded with shallow water depth and were not indicative of turbidity. The vast majority of substrate sampled was muddy sand (n = 58), followed by mud (n = 18), with one sample not evaluated. Some of the mud samples were eliminated from the analysis because they were in areas where either the reef had been scraped or where reef had not been constructed.

7.2 Oyster Size Structure

Size ranged from 3.1 to 132.2 mm SH (Shell Height = Shell Length) with most oysters being 40 to 90 mm SH (Figure 10). An adult oyster was classified as any live oyster over 35.0 mm SH. An age-0 year class, which recruited in 2018, ranged in size from 3.1 to to 35 mm SH with a mean at about 20 mm SH. Larger oysters comprised at least 2 to 3 year classes.

7.3 Oyster Density

7.3.1 Total Density per Reef Sample

Of the 68 samples taken across the reef network, 4 were in locations (Figure 11, red dots) where the reef had been scraped to translocate the oysters from unsuitable bottom to reefs on suitable bottom. The remaining 64 samples were distributed among the reef types with n = 14 for OHRR, n = 17 for OLRR and n = 31 for RHRR. All samples exceeded the GIT threshold of 15 oysters m^{-2} (Figures 11 and 12, yellow and green dots). The GIT target (50 oysters m^{-2}) was exceeded by 81% (52 of 64) of the samples.

7.3.2 Spat, Adult and Total Density

Spat density was low due to poor recruitment in 2018, inversely related to depth (Figure 13) and higher in muddy sand than in mud, but did not differ significantly by reef type (Table 2). Spat density was highest on OHRR at 43.1 m^{-2} on OHRR, intermediate on RHRR at 31.2 m^{-2}, and lowest on OLRR at 27.2 m^{-2} (Figure 13). The lack of a reef type effect resulted from the extremely poor spat set of 2018, which was due to high streamflow in 2018, and which precluded accumulation of spat on OHRR and RHRR reefs. This was also evident in the high volume of brown shell without live oysters (see below).

Adult and total density were high in 2018 and 2019, also inversely related to depth (Figures 14 and 15) and higher in muddy sand than in mud, though depth interacted significantly with reef type (Tables 3 and 4). OHRR reefs had a steeper negative slope than RHRR and OLRR reefs, such that the difference in density between OHRR and the other reef types was greatest at depths shallower than 12 feet; by 16 feet in depth, density was relatively low and differed little among the 3 reef types (Figures 14 and 15). This was

likely due to the negative effect of depth on spat recruitment in combination with effects of reef height on recruitment and survival.

To assess population-level differences in oyster density, we first determined whether depth differed by reef type. It did not (GLM, $p > 0.4$), which allowed us to generate mean population-level densities as a function of reef type (Figure 16). In contrast to spat density, both adult density and total density differed significantly by reef type (GLM, $p < 0.05$). OHRR supported the highest densities (adult: 258.9 m^{-2}; total: 301.0 m^{-2}), followed by RHRR (adult: 151.8 m^{-2}; total: 182.0 m^{-2}), and OLRR with the lowest (adult: 91.7 m^{-2}; total: 118.0 m^{-2}), though all reef types greatly exceeded the GIT target of 50 oysters m^{-2} (Figure 16).

7.4 Oyster Biomass

Total oyster biomass was high in 2018 and 2019 (Figure 17), also inversely related to depth (Figure 18) and higher in muddy sand than in mud, though depth interacted significantly with reef type (Table 5). As with adult and total oyster densities, OHRR reefs had a steeper negative slope than RHRR and OLRR reefs, such that the difference in biomass between OHRR and the other reef types was greatest at depths shallower than 12 feet; from 12 to 16 feet in depth, biomass declined and differed little among the 3 reef types (Figure 18). Given that depth did not differ by reef type, we generated mean population-level biomass as a function of reef type (Figure 19). Total biomass differed significantly by reef type (GLM, $p < 0.05$). OHRR harbored highest total biomass (173.0 g DW m^{-2}), RHRR was nearly as high (164.0 g DW m^{-2}), whereas OLRR was substantially lower (57.0 g DW m^{-2}), though all reef types exceeded the GIT target of 50 g DW m^{-2} (Figure 19).

7.5 Oyster Shell Volume

Live shell volume was high in 2018 and 2019 (Figure 20), inversely related to depth (Figure 21) and higher in muddy sand than in mud; depth again interacted significantly with reef type (Table 6). As with adult density, total oyster density and biomass, OHRR reefs had a steeper negative slope than RHRR and OLRR reefs, such that the difference in live shell volume between OHRR and the other reef types was greatest at depths shallower than 12 feet; from 12 to 16 feet in depth, live shell volume declined and differed little among

the 3 reef types (Figure 21). In contrast, brown shell volume was positively related to depth (Figure 22), did not differ by sediment type, and depth did not interact with reef type such that RHRR reefs had the highest volume of brown shell (Table 7). The change in slope with depth from negative for live shell volume to positive for brown shell volume resulted from the reduction of spat and adult densities with depth, as well as the addition of RHRR shell during reef rehabilitation.

Again, given that depth did not differ by reef type, we generated mean population-level live shell volume and brown shell volume as a function of reef type (Figure 23). Live shell volume differed significantly by reef type (GLM, $p < 0.05$). OHRR harbored highest live shell volume (8.302 L m^{-2}), RHRR was intermediate (6.650 L m^{-2}), whereas OLRR was substantially lower (2.657 L m^{-2}) (Figure 23). Conversely, brown shell volume was highest on RHRR (16.537 L m^{-2}), followed by OHRR (12.843 L m^{-2}) and then OLRR with lowest volumes (10.638 L m^{-2}) (Figure 23). When live shell volume and brown shell volume were combined by reef type, all reef types exceeded an assumed value for self-sustaining reefs of 5 L m^{-2} (Schulte et al., 2009).

7.6 Oyster Abundance

Population abundance across all reef types was estimated at approximately 76.2 million live oysters (Figure 24), most of which were adults (Figure 10). Of all oysters, OHRR reefs harbored 36.3 million, RHRR reefs 22.0 million, and OLRR reefs 17.9 million (Figure 24).

7.7 Spat Density as a Function of Adult Density

As with previous studies in the Great Wicomico River (Schulte et al., 2009) and Lynnhaven River (Lipcius et al., 2015) with sanctuary reefs, spat density was positively and significantly a function of adult density (Figure 25):

$$S = 4.20 + 176.03(1 - e^{-0.001A}) \tag{2}$$

where S = Spat density and A = Adult density.

7.8 Poaching

Poaching was evident on 6 of the 64 samples across the reef network with 3 on reef 8, 2 on reef 9 and 1 on reef 3. We identified poached samples by

the occurrence of profuse broken shell pieces and lack of large oysters either live or dead (boxes). In unpoached samples, legal-size oysters comprised a substantial portion of the population, whereas in poached samples very few oysters were of legal size. In terms of population metrics, poaching reduced biomass, adult density, oyster size and live shell volume, though it varied by reef. Poached samples also greatly reduced the number of oysters in clusters. Consistent with our predictions, brown shell volume was greater on poached samples than on unpoached samples, most likely due to the breakage of whole shells due to poaching by dredges.

8 Conclusions

- Multiple year classes inhabited the reef network, and density and biomass greatly exceeded GIT metrics. Consequently, the GWR reef network exceeds all restoration reef performance metrics established by the GIT (Figure 26).
- Accretion rates of live and brown oyster shell volume were well above those necessary for long-term, self-sustaining oyster populations.
- Despite poaching on some reefs and low spat densities reflecting poor recruitment in 2018, the sanctuary oyster reef network remains self-sustaining and resilient due to high densities of adults, biomass and accreted shell volume.
- Adaptive management whereby poorly-performing reefs were rehabilitated was successful and raised the quality of those reefs to be self-sustaining.
- The sanctuary oyster reef network harbors the longest-lasting (15 years) self-sustaining restored oyster metapopulation of any native oyster species worldwide, and serves as a model for native oyster restoration globally.

9 Tables

Table 1: **Information theoretic framework Anderson (2008) of 9 models (g_i) using water depth (D), sediment type (S) and reef type (R) as predictors of oyster density, biomass and shell volume, where k is the number of parameters in a model.**

Model number	Model	k	Description
g_1	D	3	Main effect of D
g_2	S	3	Main effect of S
g_3	R	4	Main effect of R
g_4	D + S	4	Additive model, 2 main effects
g_5	D + R	5	Additive model, 2 main effects
g_6	D * R	7	Interaction model of D and R
g_7	D + S + R	6	Additive model, all main effects
g_8	D * R + S	8	Global model
g_9	1	2	Null model

Table 2: Estimate, SE, t value and p value of the parameters from model g_7 using water depth (D), sediment type (S) and reef type (R) as predictors of spat density. The parameters are based on a log transformation. The intercept reflects the baseline condition with R = OHRR and S = Mud. Model g_7, with 59 degrees of freedom, explained 14.5% of the null deviance, whereas the best model g_4, with 61 degrees of freedom, explained 12.1% of the null deviance. Model g_7 was selected because it includes the effects of reef type.

Parameter	Estimate	SE	t value	p
Intercept (OHRR)	3.96	0.77	5.1	<<0.001
D	-0.09	0.04	-2.1	0.040
S (Muddy Sand)	0.93	0.43	2.2	0.035
RHRR	-0.41	0.33	-1.2	0.23
OLRR	-0.42	0.38	-1.1	0.28

Table 3: Estimate, SE, t value and p value of the parameters from model g_8 using water depth (D), sediment type (S) and reef type (R) as predictors of adult density. The parameters are based on a log transformation. The intercept reflects the baseline condition with R = OHRR and S = Mud. Model g_8, with 57 degrees of freedom, was the best model and explained 30.3% of the null deviance.

Parameter	Estimate	SE	t value	p
Intercept (OHRR)	7.25	0.94	7.7	<<0.001
D	-0.20	0.07	-2.7	0.010
S (Muddy Sand)	0.69	0.33	2.1	0.041
RHRR	-2.55	1.04	-2.5	0.018
OLRR	-4.30	1.32	-3.2	0.002
D * RHRR	0.17	0.08	2.1	0.043
D * OLRR	0.29	0.11	2.6	0.014

Table 4: Estimate, SE, t value and p value of the parameters from model g_8 using water depth (D), sediment type (S) and reef type (R) as predictors of total oyster density. The parameters are based on a log transformation. The intercept reflects the baseline condition with R = OHRR and S = Mud. Model g_8, with 57 degrees of freedom, was the best model and explained 30.0% of the null deviance.

Parameter	Estimate	SE	t value	p
Intercept (OHRR)	7.29	0.93	7.9	<<0.001
D	-0.20	0.07	-2.7	0.010
S (Muddy Sand)	0.78	0.33	2.4	0.020
RHRR	-2.37	1.03	-2.3	0.026
OLRR	-4.05	1.31	-3.1	0.003
D * RHRR	0.16	0.08	1.9	0.060
D * OLRR	0.27	0.11	2.5	0.017

Table 5: Estimate, SE, t value and p value of the parameters from model g_8 using water depth (D), sediment type (S) and reef type (R) as predictors of total oyster biomass. The parameters are based on a log transformation. The intercept reflects the baseline condition with R = OHRR and S = Mud. Model g_8, with 57 degrees of freedom, was the best model and explained 34.4% of the null deviance.

Parameter	Estimate	SE	t value	p
Intercept (OHRR)	6.12	0.86	7.1	<<0.001
D	-0.15	0.07	-2.3	0.028
S (Muddy Sand)	0.92	0.30	3.0	0.004
RHRR	-1.61	0.96	-1.7	0.096
OLRR	-3.69	1.21	-3.0	0.004
D * RHRR	0.13	0.08	1.7	0.100
D * OLRR	0.23	0.10	2.2	0.031

Table 6: Estimate, SE, t value and p value of the parameters from model g_8 using water depth (D), sediment type (S) and reef type (R) as predictors of live oyster shell volume. The parameters are based on a log transformation. The intercept reflects the baseline condition with R = OHRR and S = Mud. Model g_8, with 57 degrees of freedom, was the best model and explained 33.6% of the null deviance.

Parameter	Estimate	SE	t value	p
Intercept (OHRR)	10.35	0.81	12.7	<<0.001
D	-0.16	0.06	-2.4	0.018
S (Muddy Sand)	0.57	0.29	2.0	0.053
RHRR	-1.65	0.90	-1.8	0.073
OLRR	-3.43	1.15	-3.0	0.004
D * RHRR	0.12	0.07	1.7	0.102
D * OLRR	0.20	0.10	2.1	0.042

Table 7: Estimate, SE, t value and p value of the parameters from model g_5 using water depth (D) and reef type (R) as predictors of brown oyster shell volume. The parameters are based on a log transformation. The intercept reflects the baseline condition with R = OHRR. Model g_5, with 60 degrees of freedom, was the best model and explained 20.0% of the null deviance.

Parameter	Estimate	SE	t value	p
Intercept (OHRR)	8.93	0.24	36.5	<<0.001
D	0.04	0.02	2.4	0.019
RHRR	0.27	0.14	1.9	0.064
OLRR	-0.14	0.16	-0.9	0.398

10 Figures

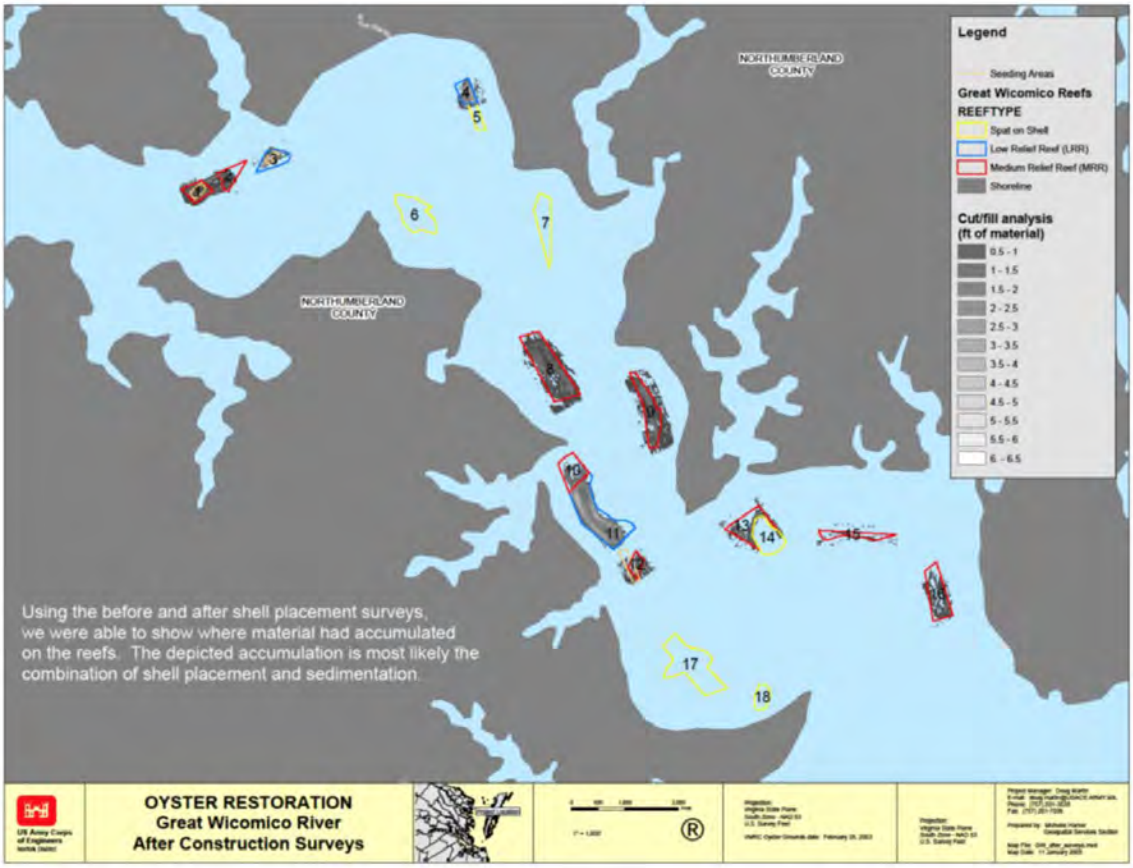

Figure 1: **Great Wicomico River showing USACE reefs.**

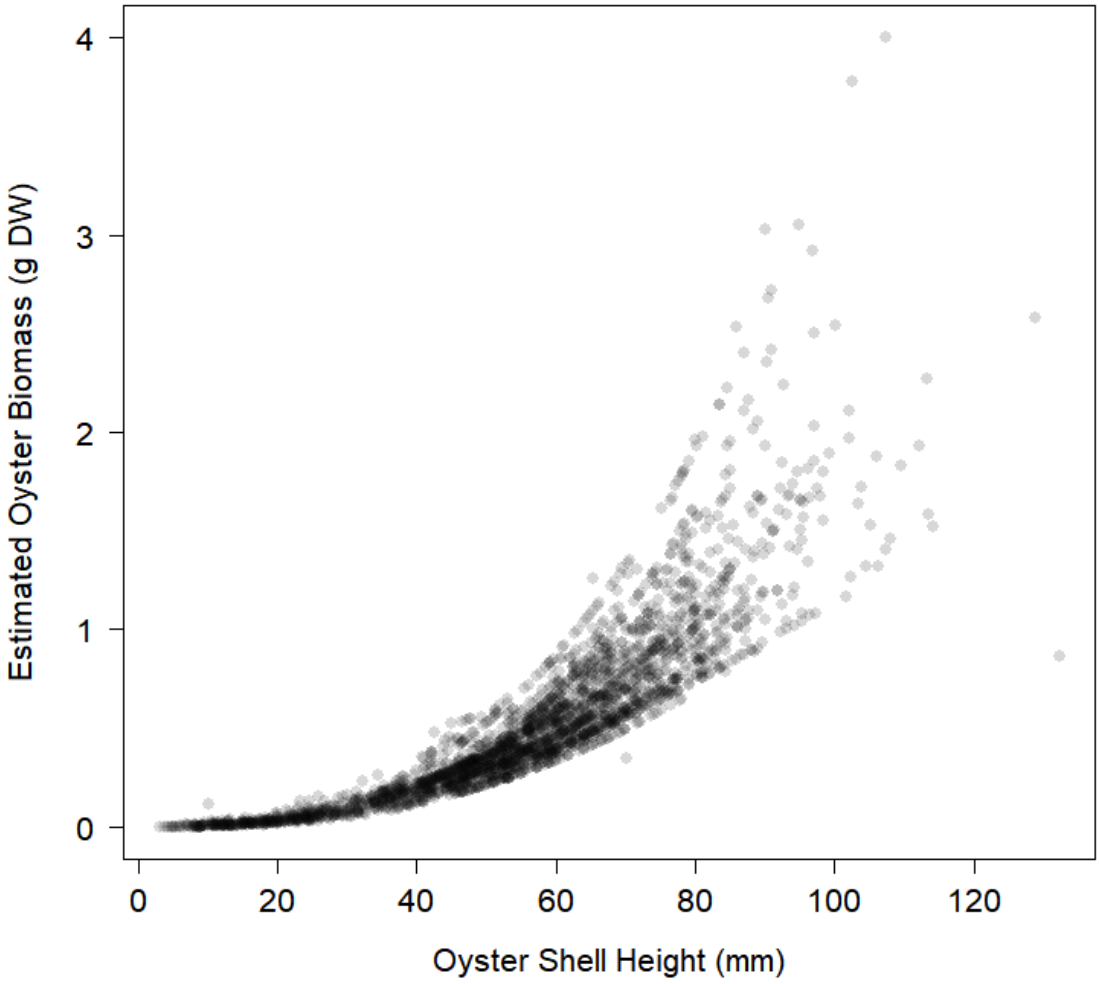

Figure 2: **All data of DW vs. SH used to generate $\log_{10}$-transformed regressions of DW vs. SH by site, reef and river.**

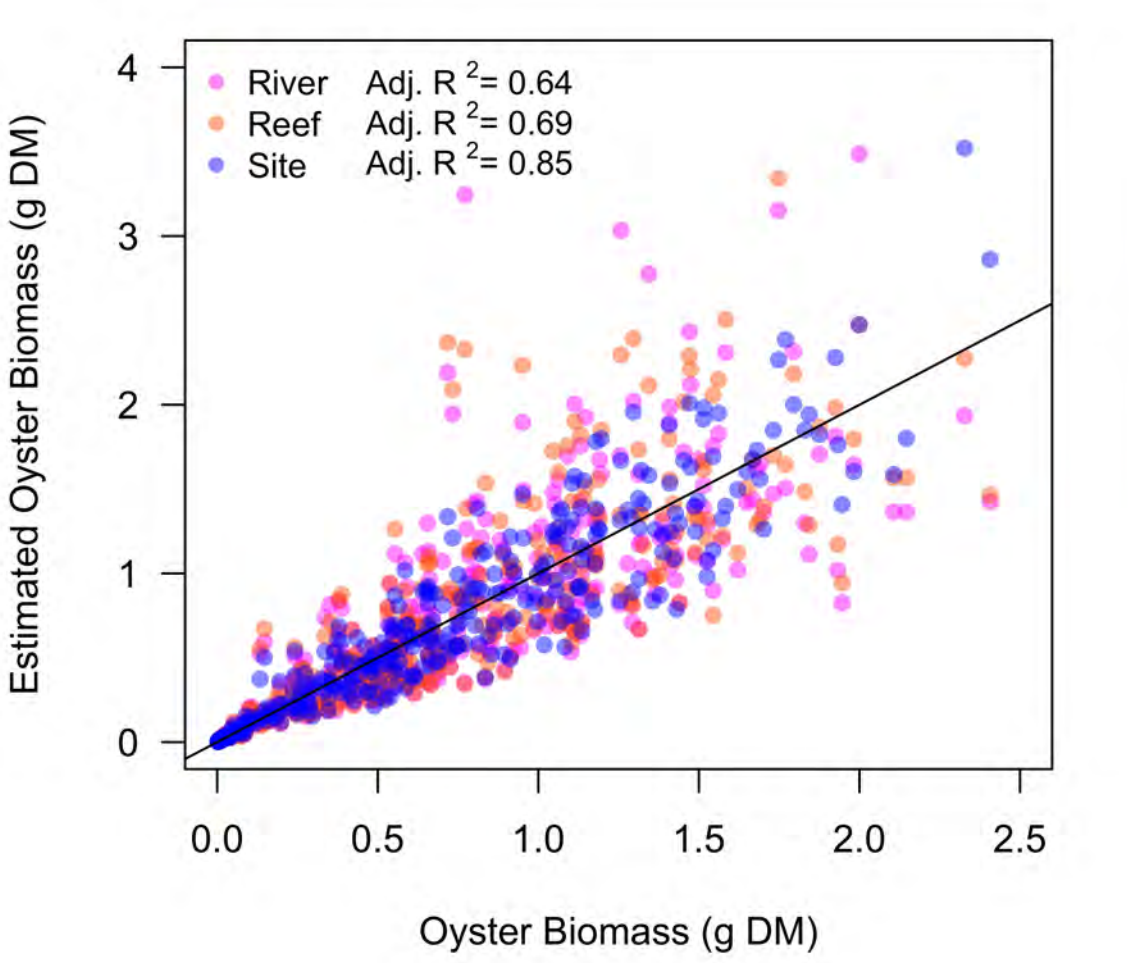

Figure 3: **Biomass regressions.**

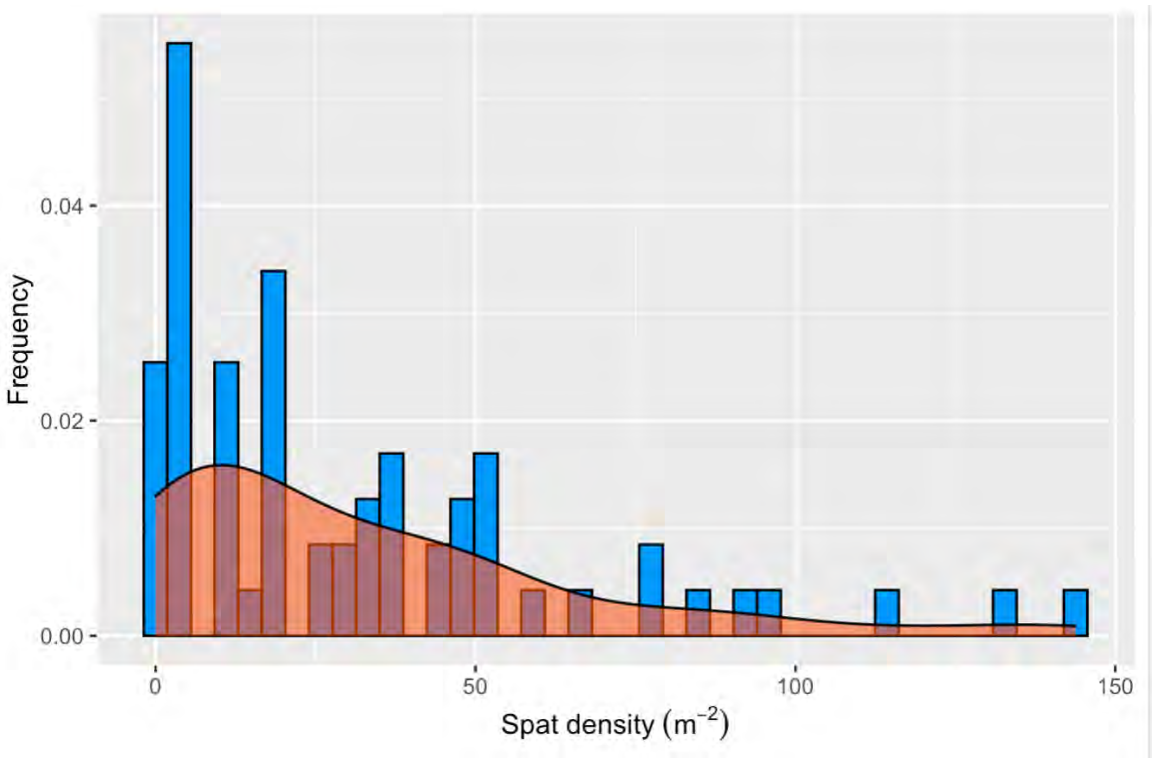

Figure 4: **Frequency histogram (blue) of spat densities. The smoothed continuous distribution is overlaid in orange.**

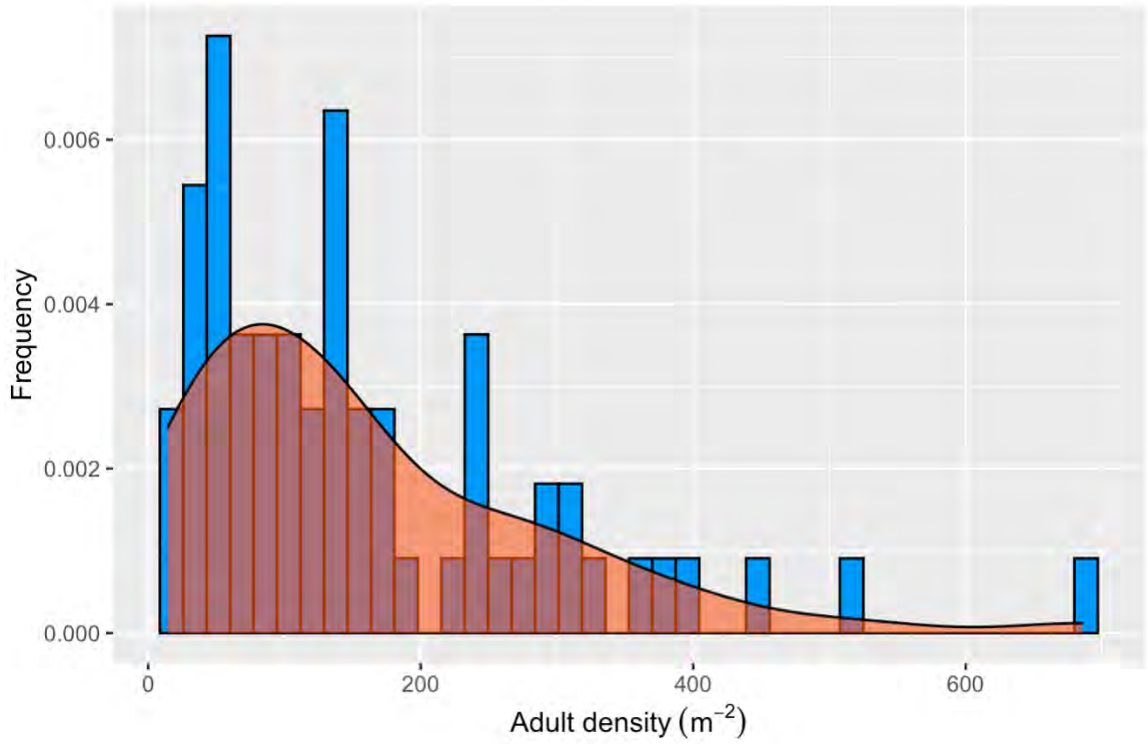

Figure 5: **Frequency histogram (blue) of adult densities. The smoothed continuous distribution is overlaid in orange.**

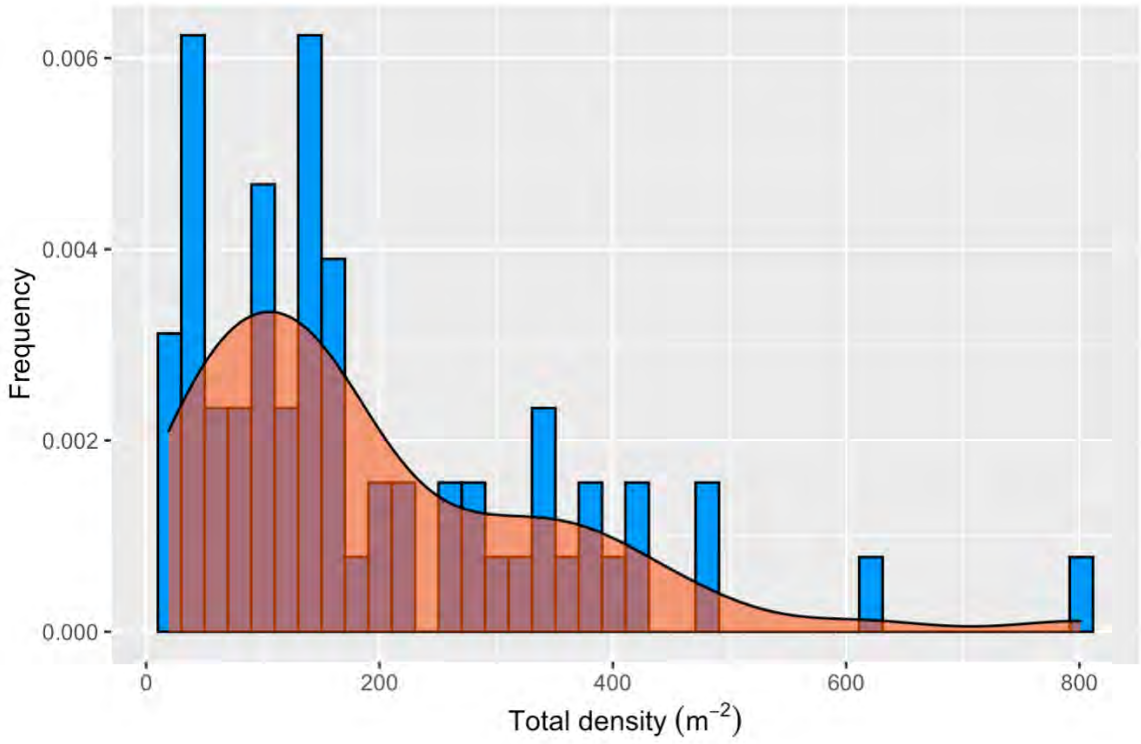

Figure 6: **Frequency histogram (blue) of total (spat + adult) densities. The smoothed continuous distribution is overlaid in orange.**

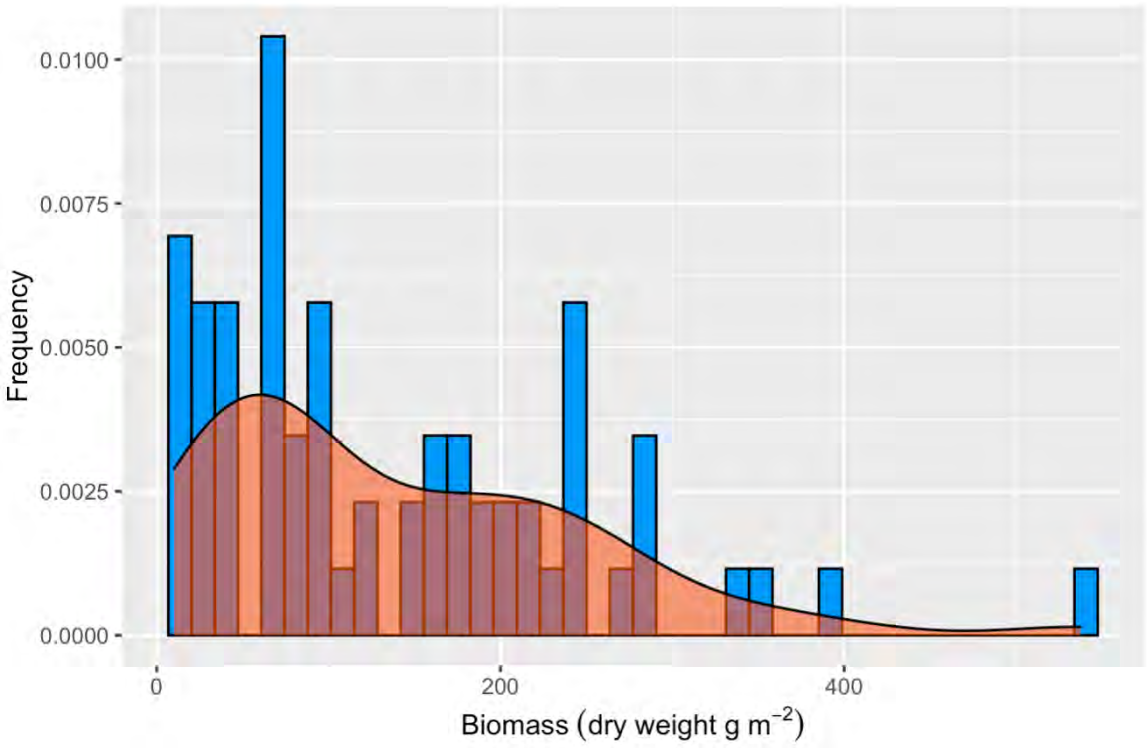

Figure 7: **Frequency histogram (blue) of total biomass values. The smoothed continuous distribution is overlaid in orange.**

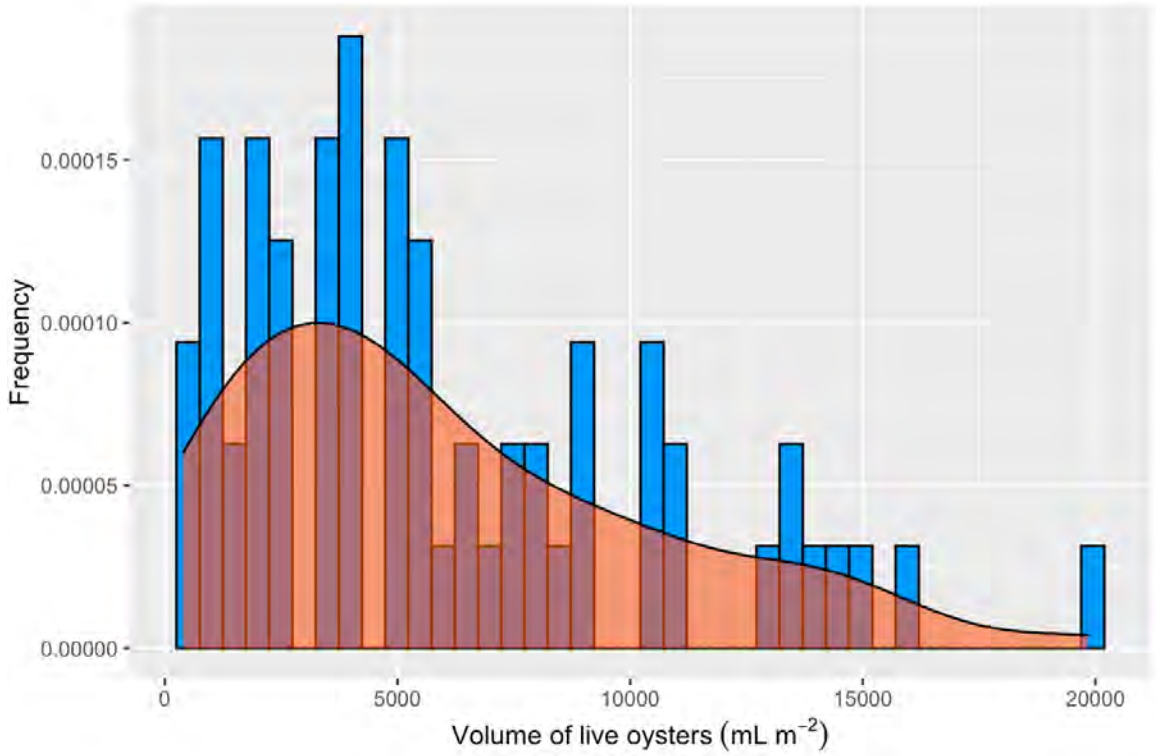

Figure 8: **Frequency histogram (blue) of live shell volumes. The smoothed continuous distribution is overlaid in orange.**

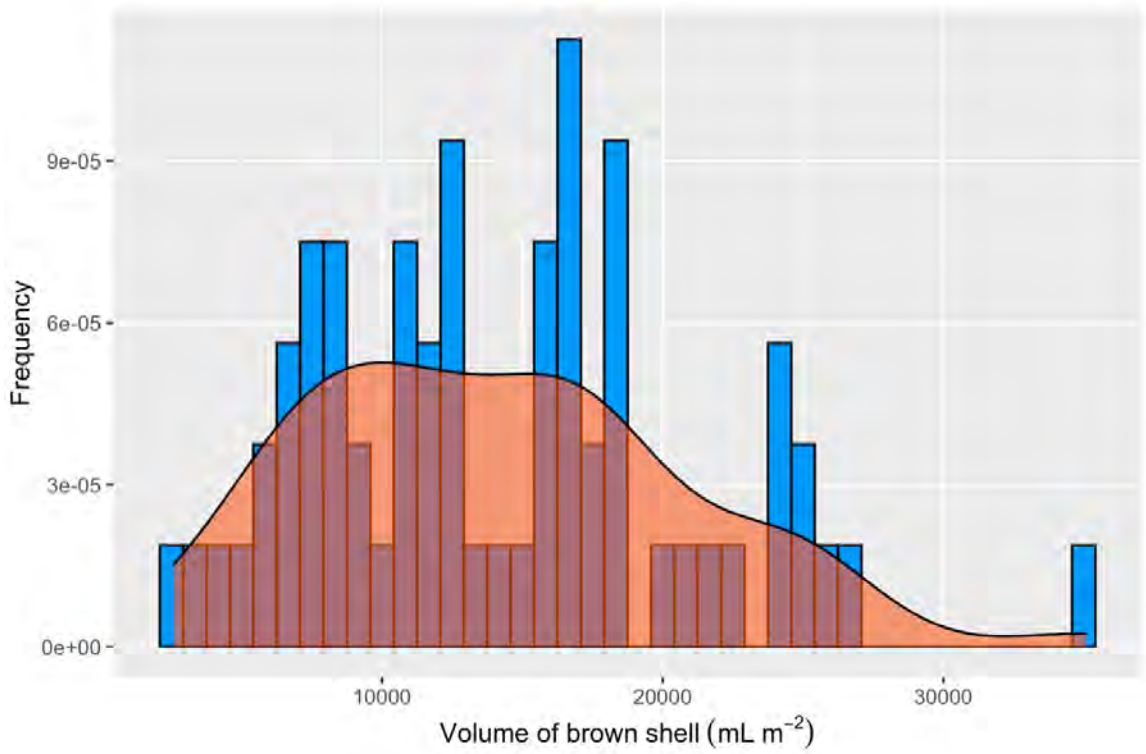

Figure 9: **Frequency histogram (blue) of brown dead shell volumes. The smoothed continuous distribution is overlaid in orange.**

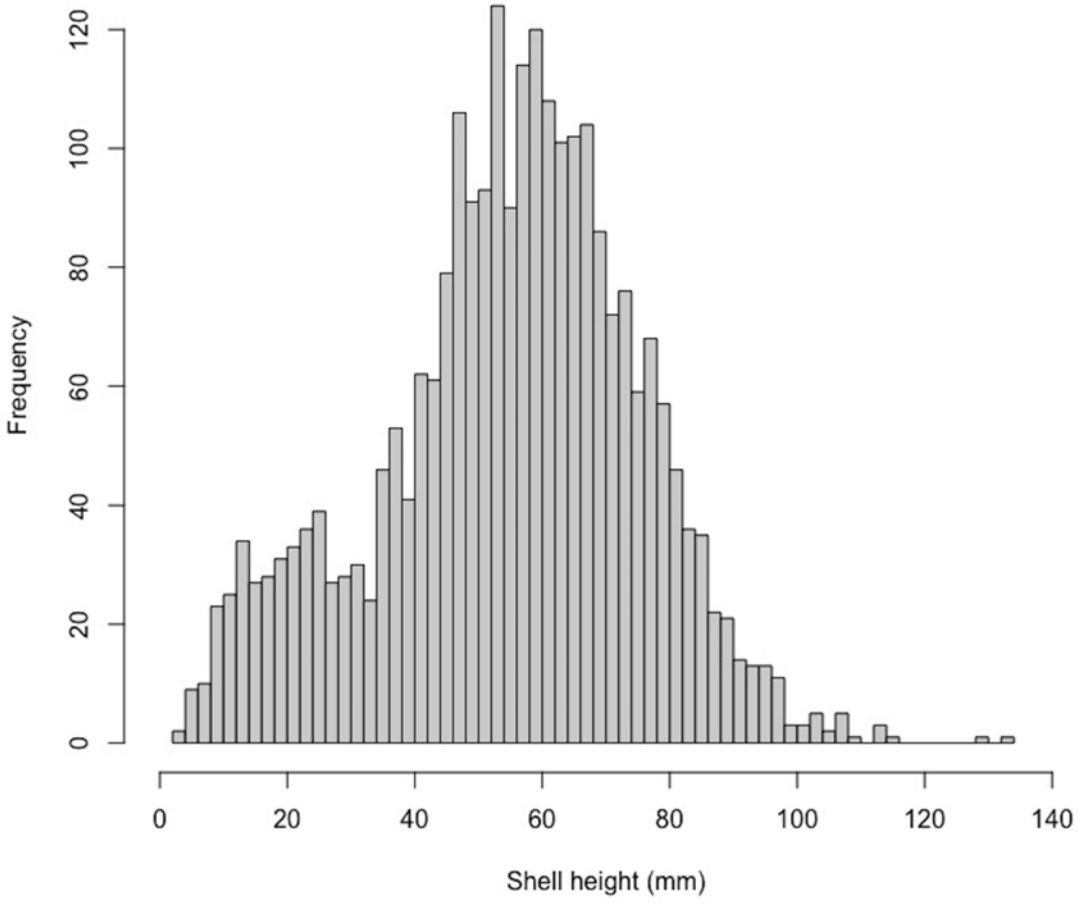

Figure 10: **Size frequencies of all oysters across the reef network.**

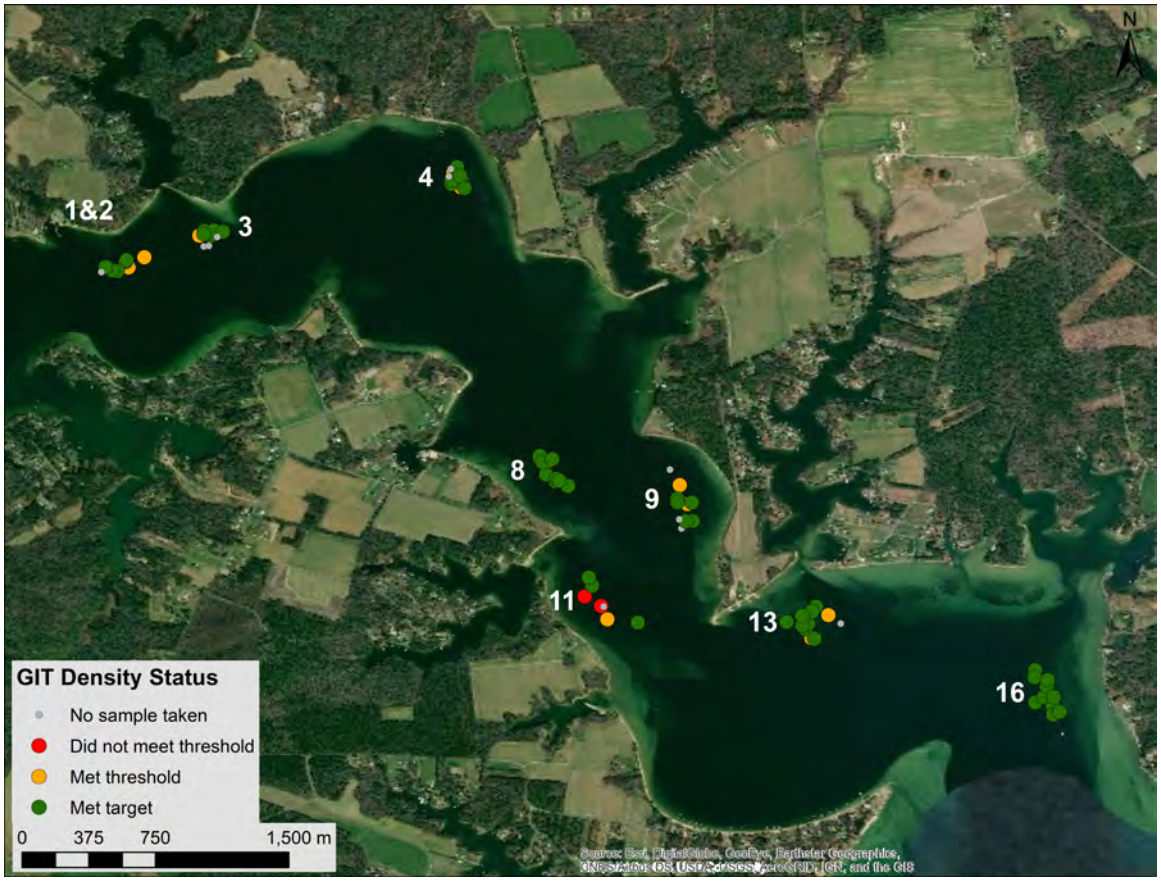

Figure 11: **Oyster density by sample.**

Figure 12: **Oyster densities for spat, sublegal and legal-size oysters by sample for each reef.**

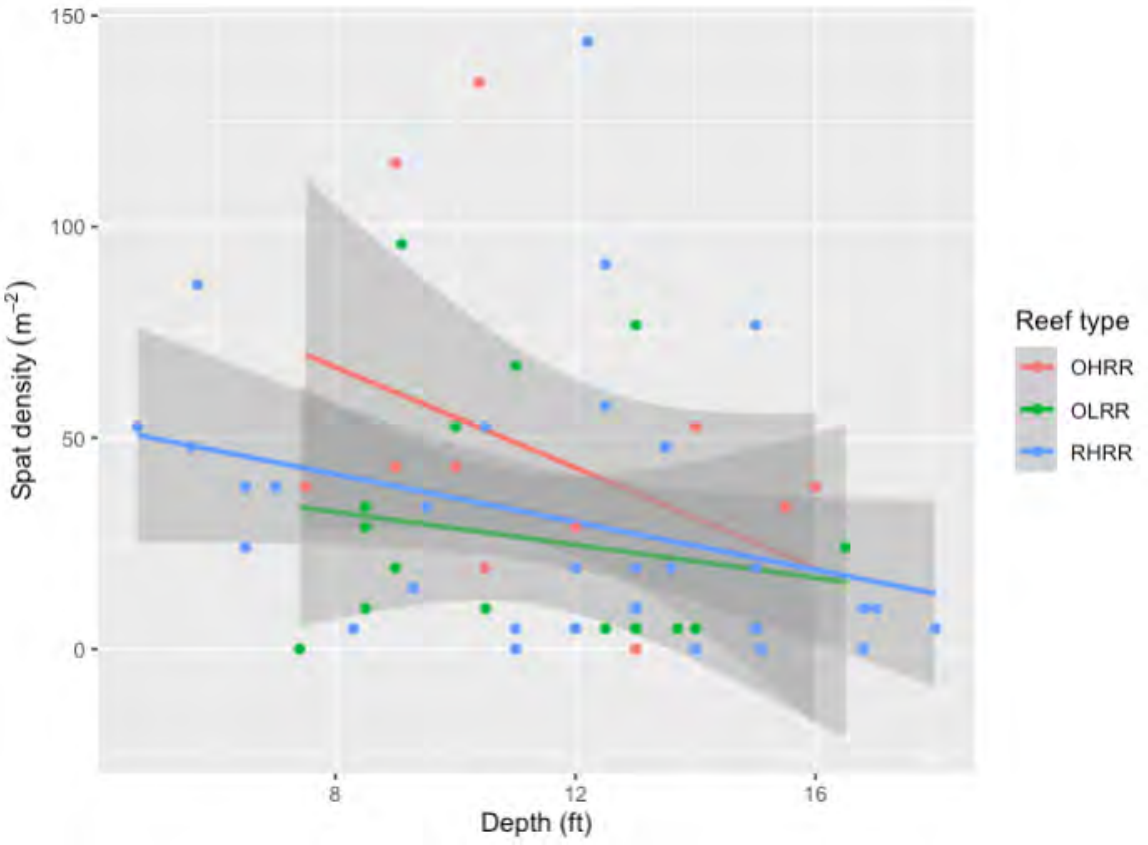

Figure 13: **Spat density by depth and reef type.**

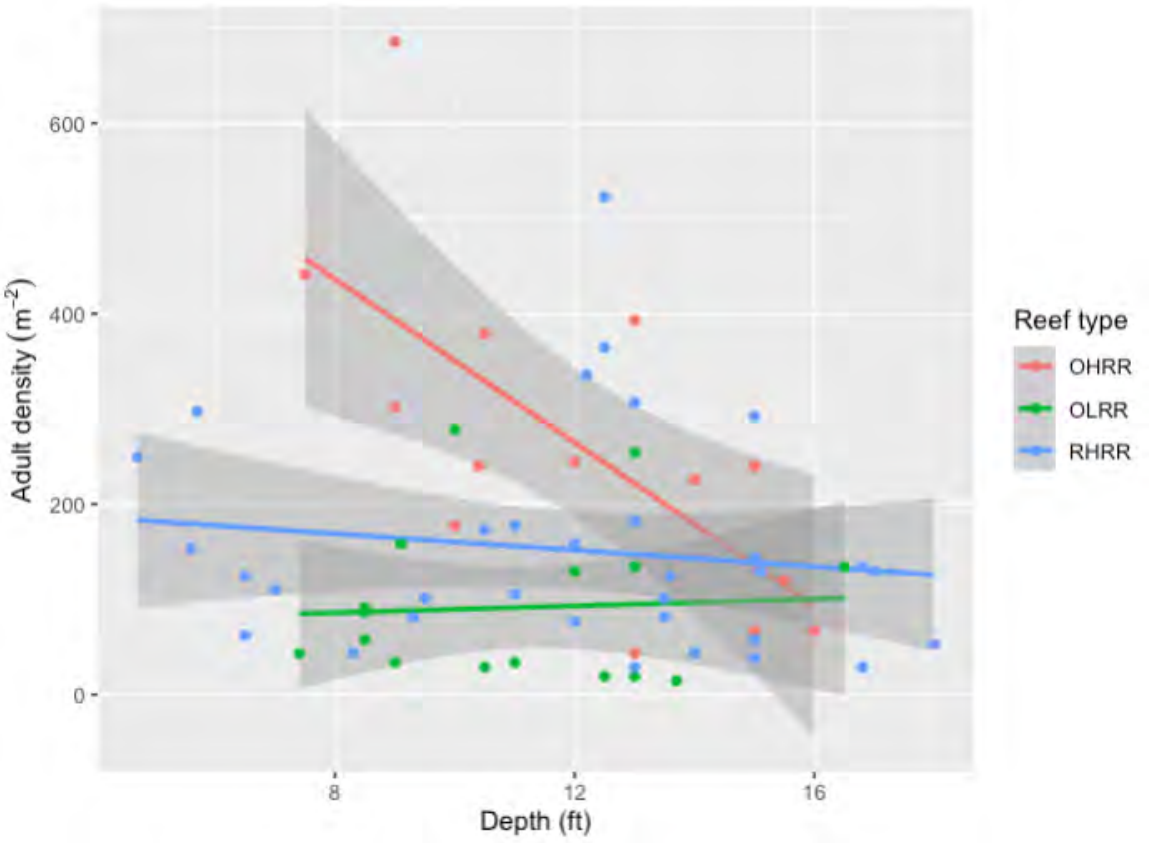

Figure 14: **Adult density by depth and reef type.**

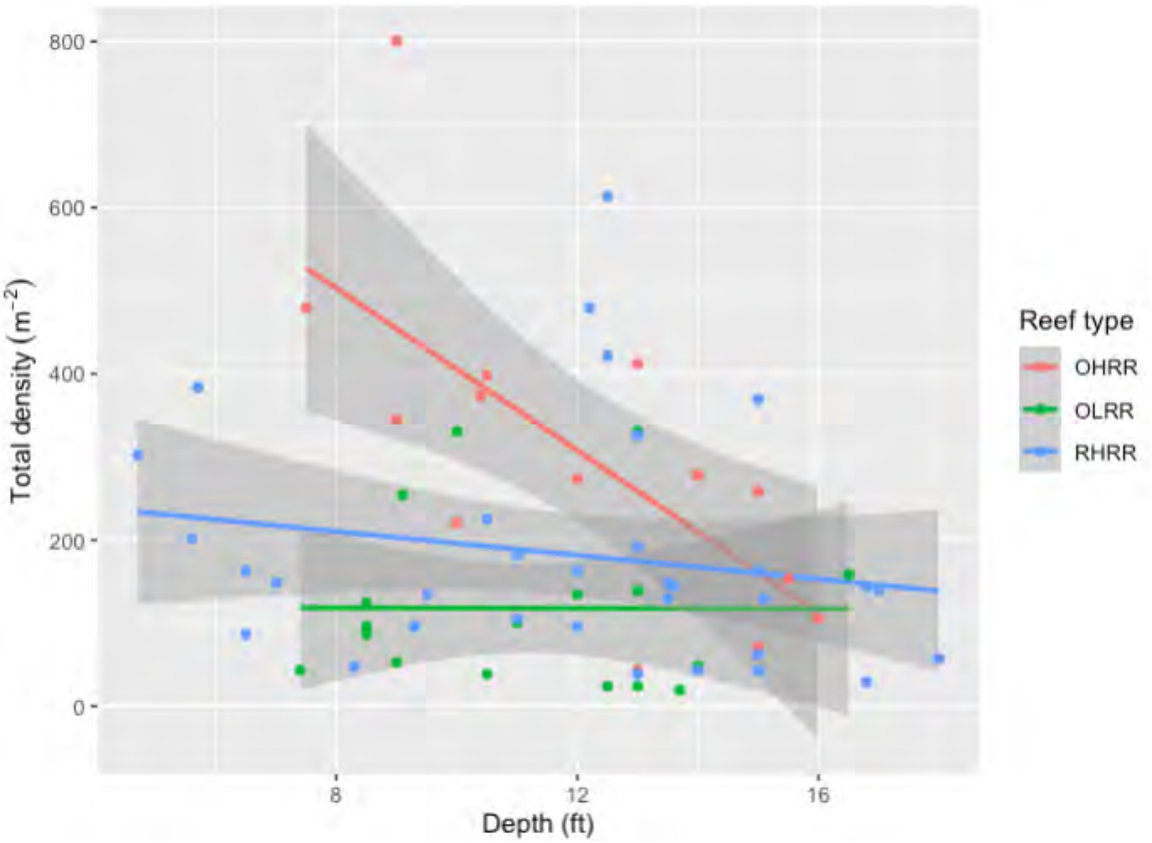

Figure 15: **Total oyster density by depth and reef type.**

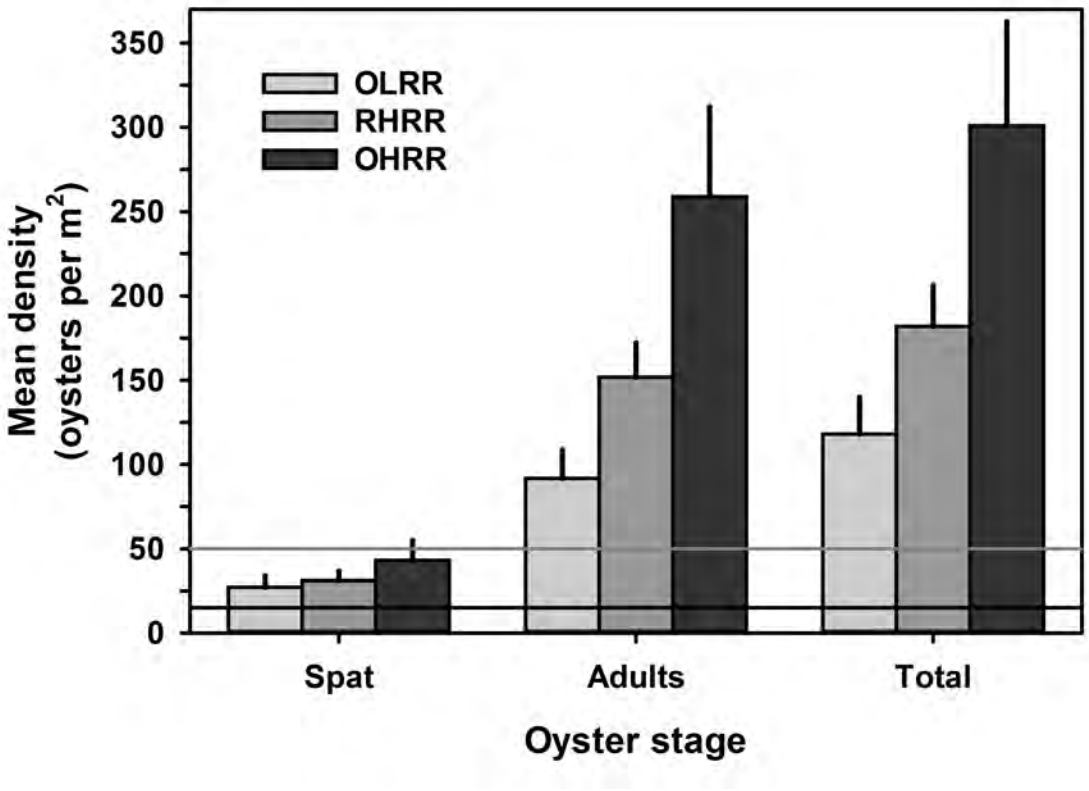

Figure 16: **Oyster density by reef type. The grey and black horizontal lines demarcate the GIT target (50 oysters per m^2) and threshold (15 oysters per m^2), respectively, for total density. Sample sizes were n = 14 for OHRR, n = 17 for OLRR and n = 31 for RHRR. Error bars represent 1 SE.**

Figure 17: **Oyster biomass by sample for each reef.**

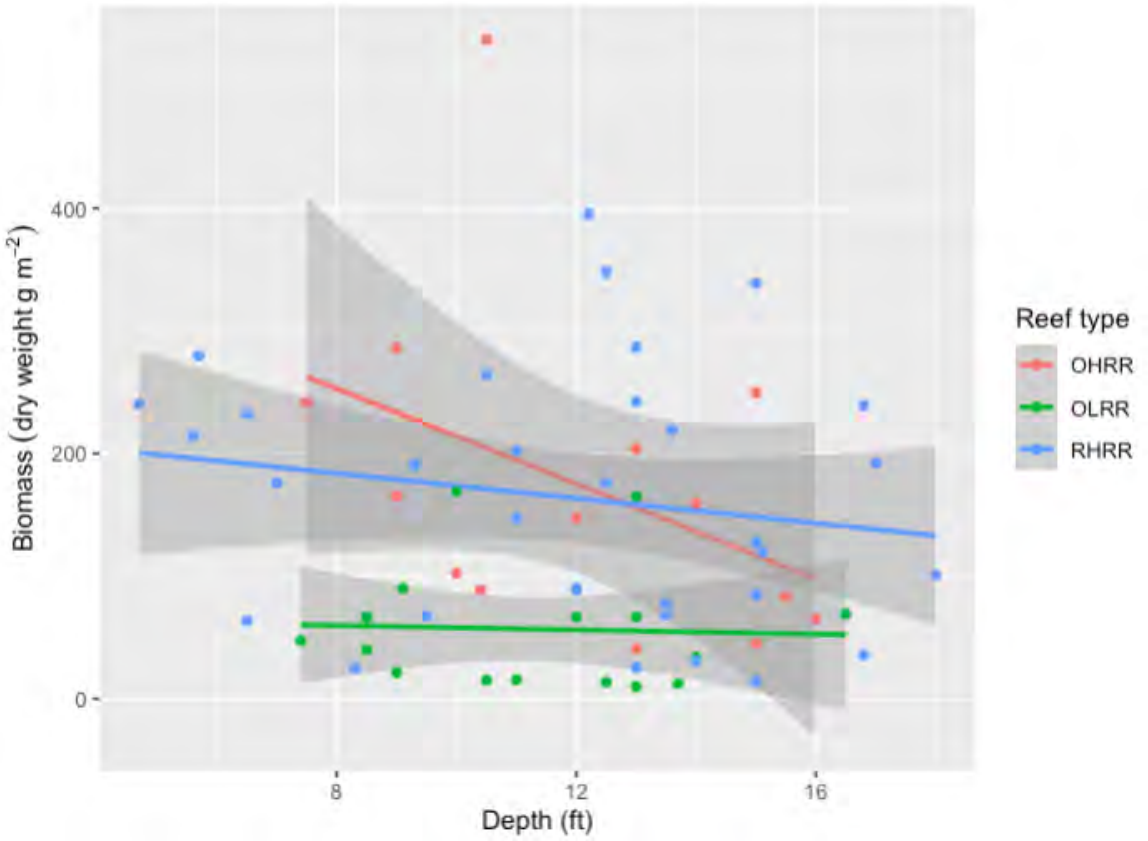

Figure 18: **Total oyster biomass by depth and reef type.**

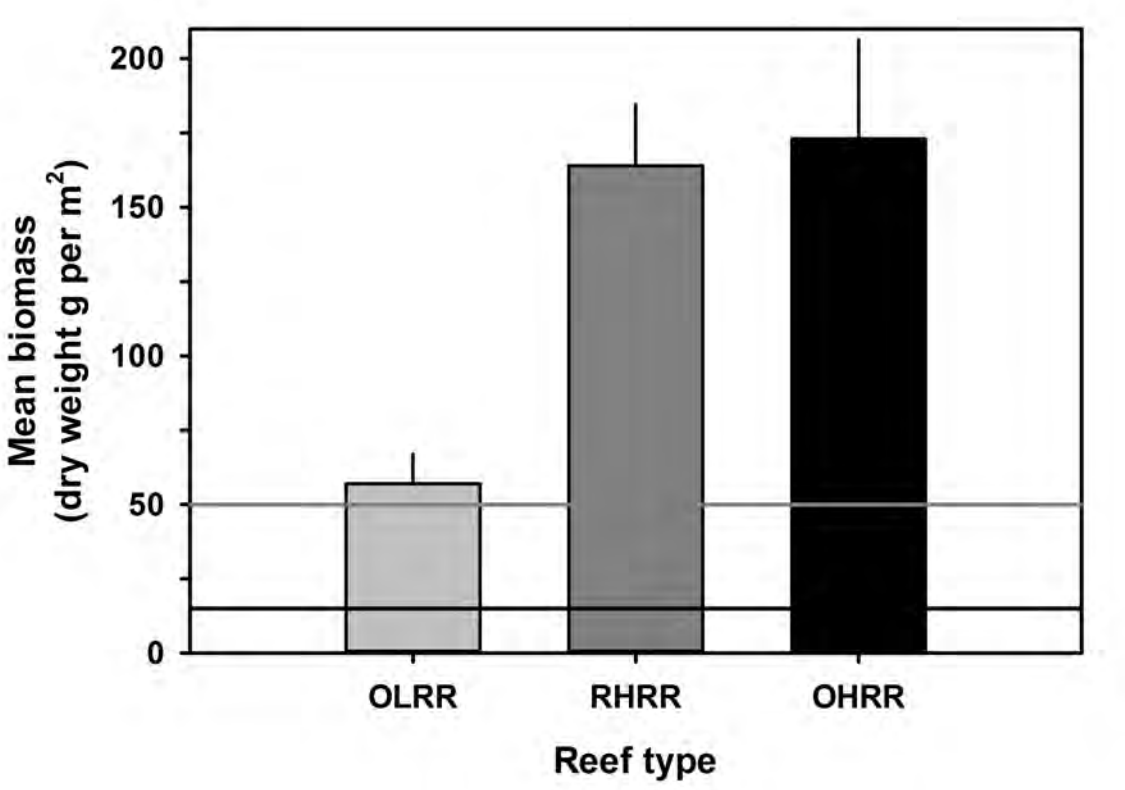

Figure 19: **Oyster biomass by reef type. The grey and black horizontal lines demarcate the GIT target (50 g dry weight per m^2) and threshold (15 g dry weight per m^2), respectively, for total biomass. Sample sizes were n = 14 for OHRR, n = 17 for OLRR and n = 31 for RHRR. Error bars represent 1 SE.**

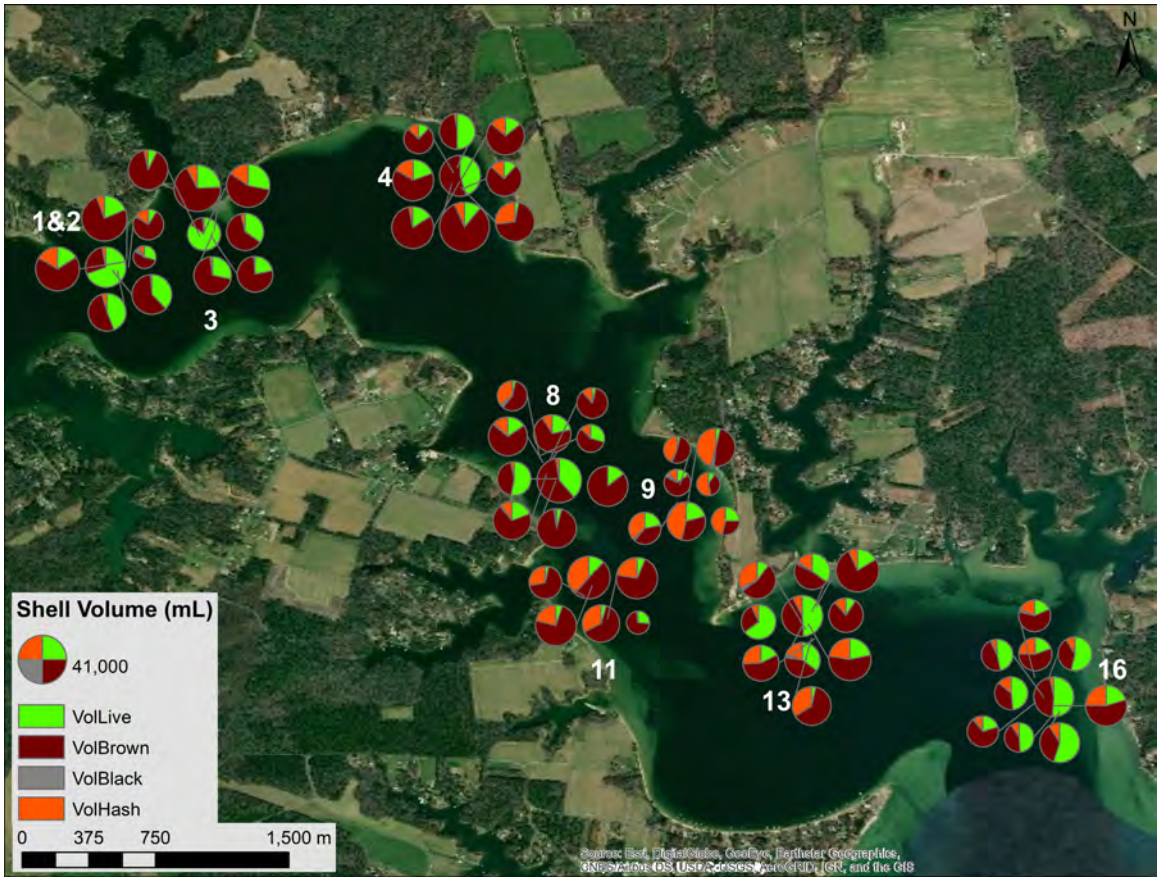

Figure 20: **Oyster volume by sample for each reef.**

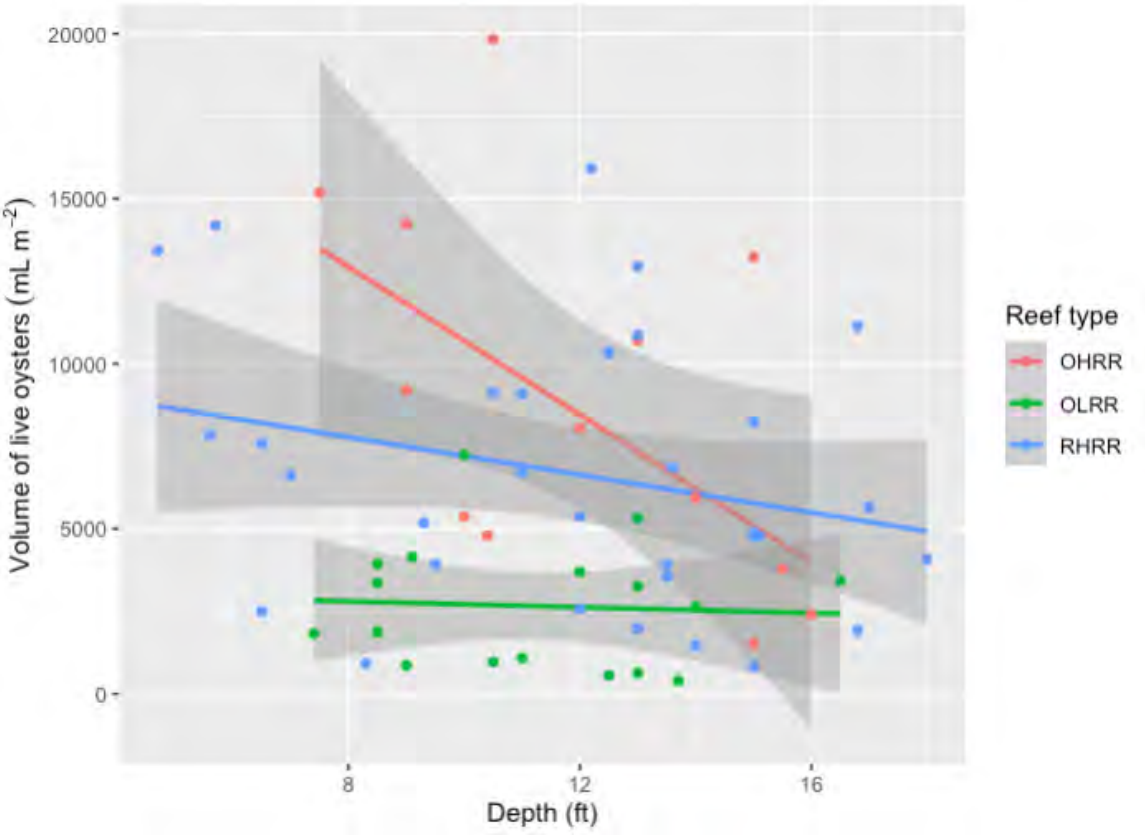

Figure 21: **Live oyster shell volume by depth and reef type.**

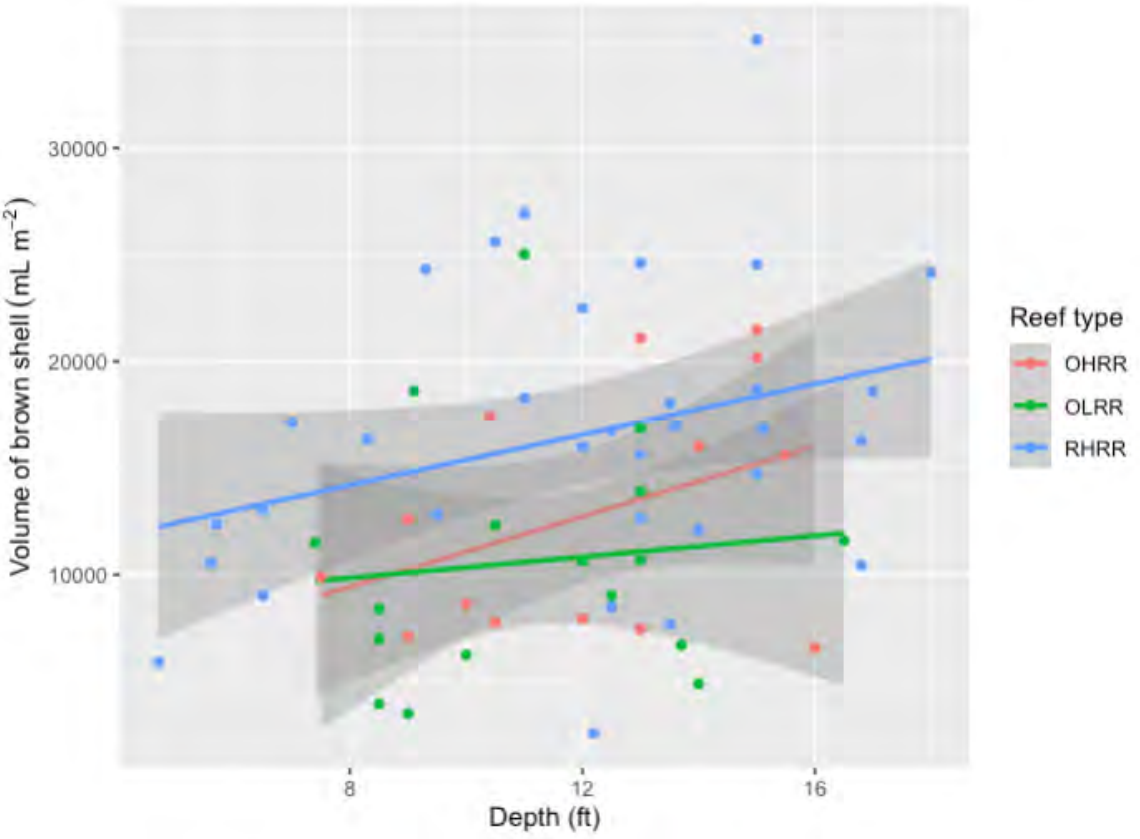

Figure 22: **Brown oyster shell volume by depth and reef type.**

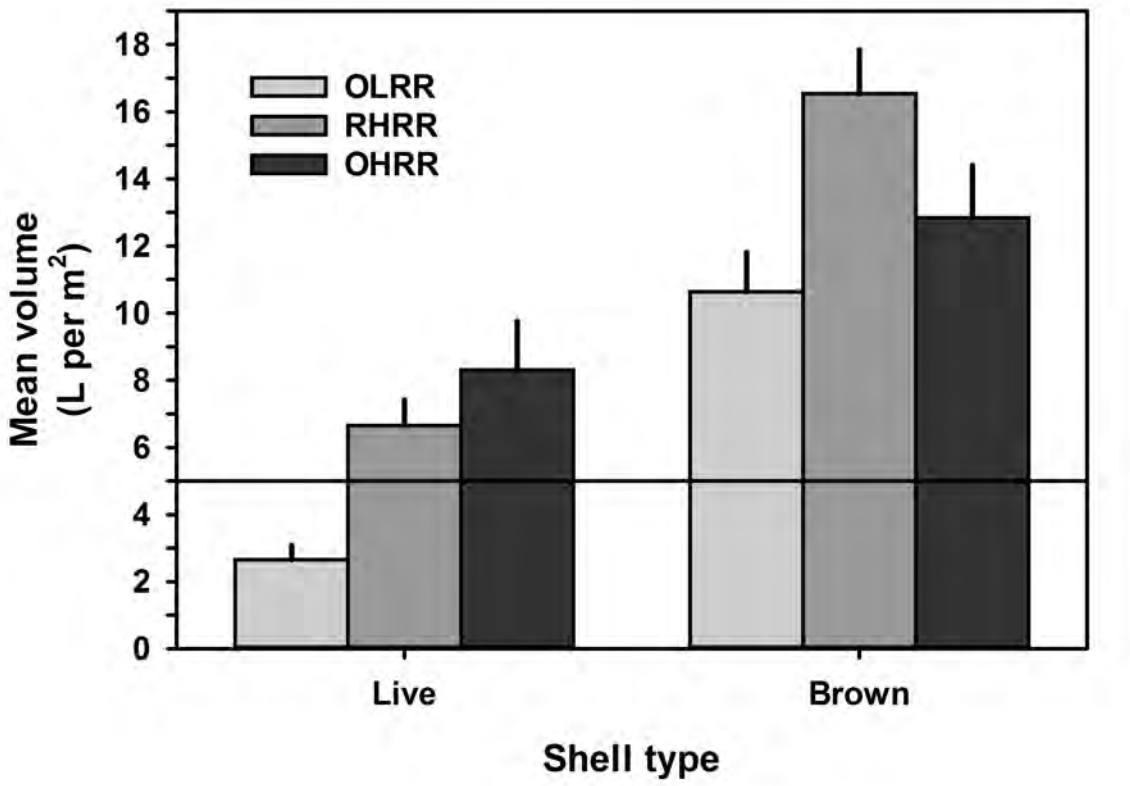

Figure 23: **Live and brown oyster shell volume by reef type. The black horizontal line demarcates an assumed value for self-sustaining reefs (5 L per m^2). Note that this value includes the sum of live and brown shell volume, such that all reef types exceeded 5 L per m^2. Sample sizes were n = 14 for OHRR, n = 17 for OLRR and n = 31 for RHRR. Error bars represent 1 SE.**

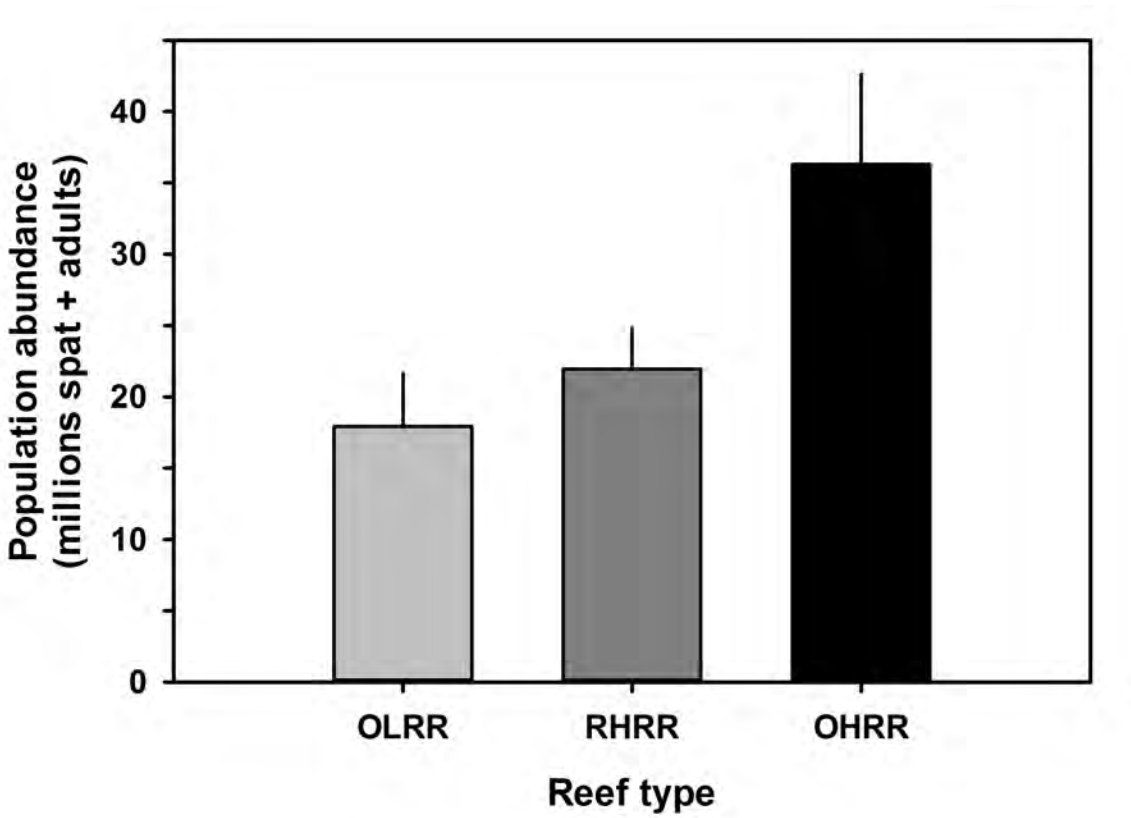

Figure 24: **Total abundance (spat + adults) by reef type. Population abundance across all reef types is estimated at approximately 76.2 million live oysters, most of which are adults. Error bars represent 1 SE.**

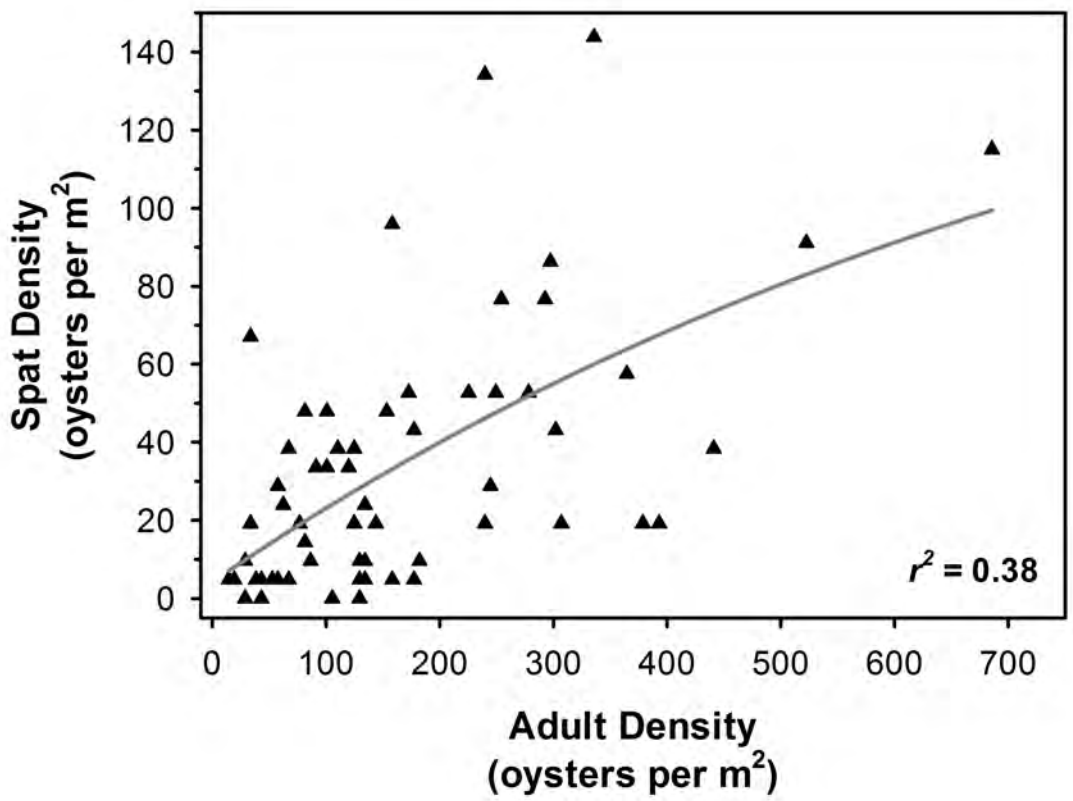

Figure 25: **Spat density as a function of adult oyster density on sampled reef patches.**

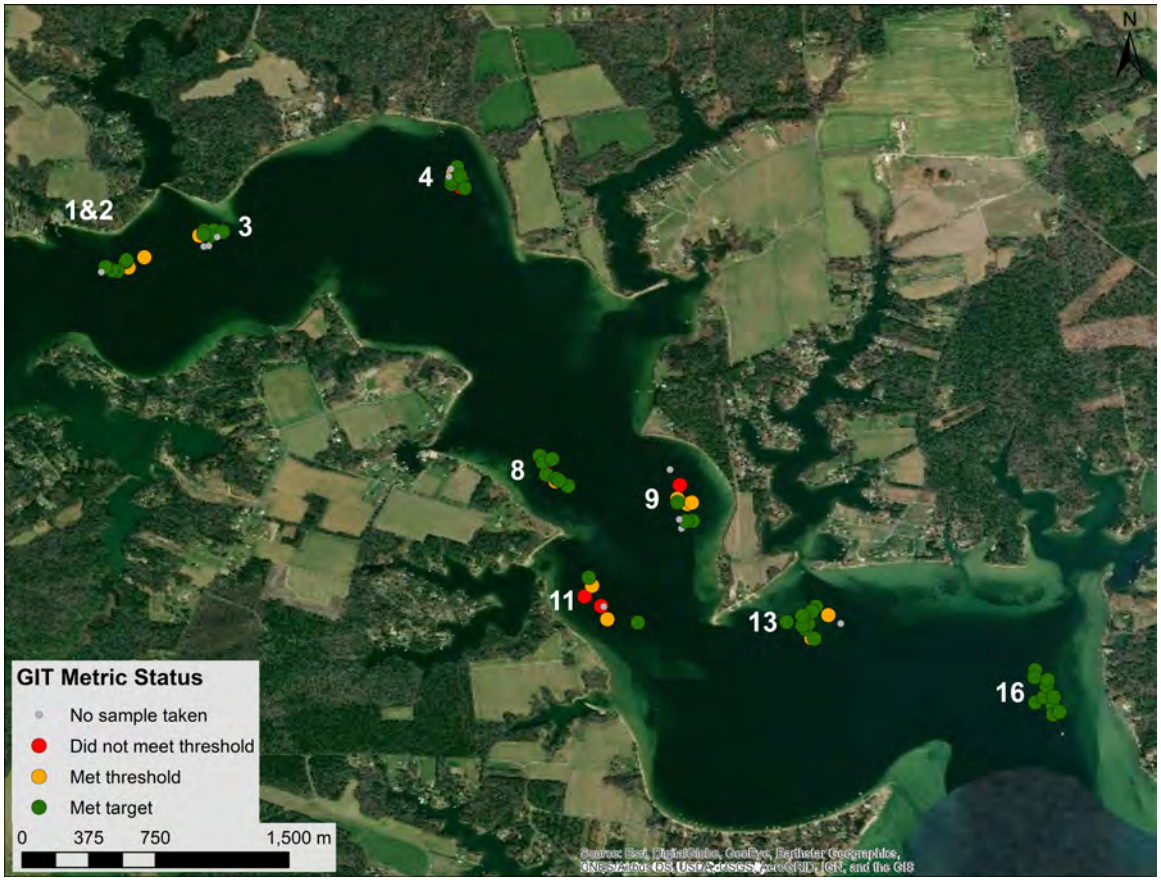

Figure 26: **GIT metrics by sample for each reef.**

11 Literature Cited

References

Anderson, D.R., 2008. Model based inference in the life sciences: a primer on evidence. Springer Science & Business Media.

Beck, M.W., Brumbaugh, R.D., Airoldi, L., Carranza, A., Coen, L.D., Crawford, C., Defeo, O., Edgar, G.J., Hancock, B., Kay, M.C., et al., 2011. Oyster reefs at risk and recommendations for conservation, restoration, and management. BioScience 61, 107–116.

Lipcius, R.N., Burke, R.P., McCulloch, D.N., Schreiber, S.J., Schulte, D.M., Seitz, R.D., Shen, J., 2015. Overcoming restoration paradigms: Value of the historical record and metapopulation dynamics in native oyster restoration. Frontiers in Marine Science 2, 65.

Lipcius, R.N., Burke, R.P., Saluta, G.G., 2020. Monitoring Oyster Restoration Reefs in the Great Wicomico, Piankatank and Lynnhaven Rivers. Chesapeake Watershed CESU W912HZ-18-SOI-0006 Final Report: Part I - Piankatank and Lynnhaven Rivers. US Army Corps of Engineers, Norfolk, Virginia. Technical Report.

Rothschild, B., Ault, J., Goulletquer, P., Heral, M., 1994. Decline of the Chesapeake Bay oyster population: A century of habitat destruction and overfishing. Marine Ecology Progress Series 111, 29–39.

Schulte, D.M., 2017. History of the Virginia oyster fishery, chesapeake bay, usa. Frontiers in Marine Science 4, 127.

Schulte, D.M., Burke, R.P., Lipcius, R.N., 2009. Unprecedented restoration of a native oyster metapopulation. Science 325, 1124–1128.

Schulte, D.M., Lipcius, R.N., Burke, R.P., 2018. Gear and survey efficiency of patent tongs for oyster populations on restoration reefs. PloS one 13.

Theuerkauf, S.J., Lipcius, R.N., 2016. Quantitative validation of a habitat suitability index for oyster restoration. Frontiers in Marine Science 3, 64.

Wilberg, M., Livings, M., Barkman, J., Morris, B., Robinson, J., 2011. Overfishing, disease, habitat loss, and potential extirpation of oysters in upper Chesapeake Bay. Marine Ecology Progress Series 436, 131–144.